# Ionization in elliptically polarized pulses: Multielectron polarization effects and asymmetry of photoelectron momentum distributions

N. I. Shvetsov-Shilovski, D. Dimitrovski, and L. B. Madsen
*Lundbeck Foundation Theoretical Center for Quantum System Research, Department of Physics and Astronomy, Aarhus University, 8000 Århus C, Denmark*
(Received 27 January 2012; published 29 February 2012)

In the tunneling regime we present a semiclassical model of above-threshold ionization with inclusion of the Stark shift of the initial state, the Coulomb potential, and a polarization induced dipole potential. The model is used for the investigation of the photoelectron momentum distributions in close to circularly polarized light, and it is validated by comparison with *ab initio* results and experiments. The momentum distributions are shown to be highly sensitive to the tunneling exit point, the Coulomb force, and the dipole potential from the induced dipole in the atomic core. This multielectron potential affects both the exit point and the dynamics, as illustrated by calculations on Ar and Mg. Analytical estimates for the position of the maximum in the photoelectron distribution are presented, and the model is compared with other semiclassical approaches.

DOI: 10.1103/PhysRevA.85.023428 PACS number(s): 32.80.Fb, 32.80.Rm, 32.80.Wr

## I. INTRODUCTION

The interaction of a strong laser field with atoms and molecules gives rise to a variety of phenomena, including above-threshold ionization (ATI) along with the formation of the high-energy plateau in the electron spectrum, excessive yield of doubly and multiply charged ions, and the generation of the high-order harmonics of the incident field (see, e.g., Refs. [1–6] for reviews). The theoretical approaches used to describe all of these phenomena are based on the numerical solution of the time-dependent Schrödinger equation (TDSE) (see, e.g., Refs. [7–11] and references therein), the strong-field approximation (SFA) [12–14], and the semiclassical model for strong-field ionization [15–19], with the initial step being tunneling ionization [20–22] and the subsequent dynamics described by classical equations of motion. When all other interactions but that of the laser field are ignored in this propagation, this latter approach is known as the simpleman's model.

Although the solution of the TDSE in most cases gives good agreement with the experimental data, it is often very difficult to reconstruct the mechanism of the phenomena under consideration. In the SFA the initial bound state of the atom is unaffected by the laser field, whereas the final continuum state does not feel the binding potential of the parent ion. Despite the appealing physical picture of many laser-atom phenomena provided by the SFA, it has been known for many years that neglecting the binding potential is severe [23–31].

The three-step model [15–19] has given great insight into strong-field phenomena. Presently semiclassical simulations based on the three-step model are widely used due to (i) their numerical simplicity and (ii) the physical picture of strong-field phenomena. For some laser-atom problems, the semiclassical simulations are, in fact, the only feasible approach, for example, for the nonsequential double ionization of molecules [32] and atoms by elliptically [33–36] and circularly polarized fields [37]. For a linearly polarized field the three-step model is equivalent to the following simple picture. At some time an electron tunnels out of the atom and moves along a classical trajectory in the laser field. The tunneling rate is calculated in the static limit [20] with a field strength set equal to the instantaneous value of the oscillating laser field. The description of the ionization step by tunneling is expected to be accurate when the Keldysh parameter $\gamma = \omega\varkappa/F \ll 1$ [12], where $\omega$ is the carrier angular frequency, $F$ is the field strength, and $\varkappa = \sqrt{2I_p}$ with $I_p$ the ionization potential (atomic units are used throughout this paper). In most cases the tunneled electrons reach the detector without recolliding with their parent ions. These direct electrons have energies below $2U_p$, where $U_p = F^2/4\omega^2$ is the ponderomotive energy. There are also electrons which are driven back by the laser field to rescatter on their parent ions by angles close to 180°. These backscattered electrons are responsible for the formation of the high-energy plateau of the ATI spectrum, which is usually 4–6 orders of magnitude lower than the maximum of the low-energy spectrum. In this work we focus on the direct electrons, that is on the low-energy spectrum, therefore the model that we use consists of essentially two steps: Ionization and propagation. In the following we shall refer to this situation where recollision has been switched off as the two-step model. An example where recollision is absent is the case of ionization in close to circularly polarized fields considered here.

Above-threshold ionization, as well as other strong-field phenomena generated by elliptically polarized fields, has attracted particular attention for a number of reasons. First, the evolution of the distributions with increasing ellipticity from linear to circular gives additional information about the process under consideration. Second, in the experiment it is easier to control the ellipticity than the intensity of the fluctuating laser pulse. Finally, the kinematics caused by an elliptically polarized field is essentially two dimensional (2D), in contrast to the case of linear polarization, when the laser field acts only along one spatial direction. The 2D nature, in turn, gives rise to features and properties which are not accessible with a linearly polarized laser field. For example, the ATI by a circularly polarized laser pulse was used in the first observation of the carrier-envelope effect in [38], see also theoretical studies [39,40].

Another example is the angular distribution of photoelectrons generated by an elliptically polarized field. While

 

the SFA predicts a fourfold symmetry of the photoelectron angular distribution with respect to the both main axes of polarization ellipse [41], the experimentally observed distributions possess only inversion symmetry, see Refs. [23–25]. This was soon realized to be an effect of the Coulomb potential [26–28,42–44]. Other examples are the predominant ionization when the field points along the major axis resulting in peaks in the photoelectron momentum distribution along the minor axis [41,45,46], asymmetries in the photoelectron angular distributions resulting from the ionization of the oriented molecules [47–52], attosecond angular streaking [53,54], and the possibility of detailed exploration of Stark and polarization effects in the initial tunneling step [55].

In Ref. [56] the molecular SFA was extended to include the linear and quadratic Stark shifts. The adiabatic approximation was made in order to find the effective potential for the outer electron, which includes the laser field and the polarization effects of the inner core. It was found in Ref. [55] that the parabolic coordinates approximately separate the Schrödinger equation with this effective potential. This separation procedure defines a certain tunneling geometry, that is, identifies the flow of the electron charge associated with the tunneling electron in parabolic coordinates. The emerging physical picture is referred to as tunnel ionization in parabolic coordinates with induced dipole and Stark shift (TIPIS). Here we describe the TIPIS model and explore its predictions.

In the study of Ref. [55] the offset angle $\theta$, that is, the angle between the maximum of the momentum distribution and the minor axes of the polarization ellipse (see Fig. 1), was in focus. It was found that for Ar in the tunneling regime this angle is of the order of 10°–15° and decreasing with laser intensity, whereas for He the angle was 5°–10° and less sensitive to the laser intensity. The difference between Ar and He was related to the difference in polarizability of the two systems. It is interesting to find a situation where the offset angle is larger, that is, the effect of rotation away from the minor axis is more pronounced. Here we consider not only the offset angle, but the shape of the whole distribution and its evolution with the intensity and wavelength.

In this paper we (i) present an exhaustive derivation of the TIPIS model; (ii) validate the semiclassical approach by comparing with TDSE results; (iii) analyze momentum distribution generated by an elliptically polarized laser field; (iv) further investigate the role of the polarization effects; and (v) compare different approaches to the semiclassical simulations of the ATI.

The paper is organized as follows. In Sec. II we discuss approaches to the classical simulation of the momentum distribution, present a detailed derivation of the TIPIS model, and discuss its range of applicability. Our results are discussed in Sec III and conclusions are given in Sec. IV.

## II. SEMICLASSICAL MODELS

In the semiclassical approach to ATI, the electron is ejected from the atom by tunneling [20–22]. Subsequently, Newton's equations of motion are solved for the electron, starting out at the exit of the tunnel in the combined atomic or ionic potential $V(\mathbf{r})$ and the electric field $\mathbf{F}(t)$ of the laser pulse,

$$\frac{d^2\mathbf{r}}{dt^2} = -\nabla V(\mathbf{r}) - \mathbf{F}(t). \tag{1}$$

Semiclassical models have been successfully used to explain various strong-field phenomena involving single ionization (see, e.g. [55,57–64]) and double ionization [34–37,65,66]. The abovementioned models vary greatly with respect to the particular implementation. Here we present the semiclassical model referred to as TIPIS [55].

To solve Eq. (1) one needs to specify the initial conditions for the electron in phase-space just after the escape from the atom. The static tunneling rate with which the classical trajectories are weighted is a quantum input in the semiclassical model. The exit point at the outer turning point of the barrier also depends critically on the quantum model used to solve the tunneling problem—a key point that we come back to below. To start, we consider the static problem of an electron, bound by $V(\mathbf{r})$ in the presence of the static electric field $\mathbf{F}$ (which should be interpreted as the instantaneous value of the laser field at the time of ionization and it is assumed to point in the positive $z$ direction) [67],

$$\left(-\tfrac{1}{2}\Delta + V(\mathbf{r}) + \mathbf{F}\cdot\mathbf{r}\right)\Psi = -I_p(F)\Psi. \tag{2}$$

In Eq. (2) we have included the static Stark shifts [50,56],

$$I_p(F) = I_p(0) + \tfrac{1}{2}(\alpha_N - \alpha_I)F^2, \tag{3}$$

where $I_p(0)$ is the field-free ionization potential and $\alpha_N$ and $\alpha_I$ are the static polarizabilies of the atomic system with charge $Z-1$ and the $Z$-charged atomic ion, respectively. We have specialized to the case of atoms, with no permanent dipole moment and therefore no linear Stark shift is present in Eq. (3). The above perturbative expansion of the Stark-shifted ionization potential holds for shifts that are small compared to the field-free ionization potential $I_p(0)$. In all cases presented in this paper, this requirement is satisfied.

Following the ionization step, we will consider propagation in the potential $V(\mathbf{r})$,

$$V(\mathbf{r},t) = -\frac{Z}{r} - \frac{\alpha_I \mathbf{F}(t)\cdot\mathbf{r}}{r^3}, \tag{4}$$

which is valid at large and intermediate distances [56,67], and where the multielectron effect expressed through the induced dipole of the ion $[\alpha_I \mathbf{F}(t)]$ is taken into account [55,56]. We refer to the second term of Eq. (4) as the multielectron (ME) term.

In semiclassical simulations it is important to find the tunnel exit point $z_e$, from where the classical trajectory starts. In the next two subsections we present two possible approximate separations of the static tunneling problem that lead to different values of the tunnel exit point, and therefore different results in the semiclassical model.

### A. Field direction model

The simplest and most widely used approach to determine the tunneling path and $z_e$ is to consider the potential barrier formed by the atomic potential and the electric field of the laser in a 1D cut *along the direction of the field*. We denote

this approach as the field direction model (FDM) (see, e.g., Refs. [57,58,63,68,69]), where this model was used. The tunnel exit point is found from

$$V(z_e) + Fz_e = -I_p(F). \tag{5}$$

However, in this approach, it is implicitly assumed that the tunneling problem can be treated as one dimensional along the field direction. The direction along the field can be separated from the transverse coordinates in Eq. (2) if the potential does not depend on the transverse dimension, that is when $V(\mathbf{r}) = V(z)$. Then the wave function can be sought as a product $\Psi(x,y,z) = \Psi_2(z)\Psi_1(x,y)$, and Eq. (2) is separated as follows:

$$-\frac{1}{2}\left(\frac{\partial^2}{\partial x^2} + \frac{\partial^2}{\partial y^2}\right)\Psi_1(x,y) = \lambda_1\Psi_1(x,y), \tag{6}$$

$$\lambda_1 = \frac{p_x^2 + p_y^2}{2} = \frac{p_\perp^2}{2}, \tag{7}$$

$$\left(-\frac{1}{2}\frac{\partial^2}{\partial z^2} + V(z) + Fz\right)\Psi_2(z) = \lambda_2\Psi_2(z), \tag{8}$$

where $\lambda_1$ and $\lambda_2$ are the separation constants. The sum of the separation constants is equal to the energy of the initial state

$$\lambda_1 + \lambda_2 = -I_p(F), \tag{9}$$

and therefore

$$\lambda_2 = -\left(I_p(F) + \frac{p_\perp^2}{2}\right). \tag{10}$$

Equation (6) states the fact that because the artificial potential used in the FDM does not depend on the transverse dimension, the electron can be described as a free particle in these degrees of freedom. On the other hand, Eq. (8) gives the effective 1D tunneling problem where Eq. (10) shows that the effective ionization potential is increased by the transverse kinetic energy of the particle [70]. The minimal ionization potential that occurs for transverse energy zero is taken into the equation for the tunnel exit point in FDM (5).

It is clear that the potential in Eq. (4), even without the ME term, is not in the form required for a separation in the FDM. A much more accurate approach is to use parabolic coordinates as discussed in the next subsection.

### B. Separated problem in parabolic coordinates and TIPIS model

To separate the problem of an electron bound by a pure Coulomb potential in a static field, parabolic coordinates are used [20]:

$$\xi = r + z, \quad \eta = r - z, \quad \phi = \arctan(y/x). \tag{11}$$

Under the assumption that the electric field vector points in the positive $z$ direction, the separation results in two 1D problems: in the $\xi$ coordinate the electron is trapped in an attractive potential without the possibility to tunnel out, whereas in the $\eta$ coordinate a potential barrier exists that enables tunneling [20]. However, for the potential in Eq. (4), where the ME term is included, and also, in general for atomic and molecular potentials, such a separation is not possible. In Ref. [55] an *approximate* separation in the limit $\xi/\eta \ll 1$ was carried out. As the external field is increased, the exit point moves to smaller distances. Hence, the approximate separation becomes inaccurate if the field strength becomes too large.

To perform the separation we seek the solution to Eq. (2) in the product form $\Psi(\mathbf{r}) = (1/\sqrt{\xi\eta})f_1(\xi)f_2(\eta)e^{im\phi}/\sqrt{2\pi}$, and after retaining the lowest-order term in $\xi/\eta$ coming from $\alpha_I\mathbf{F}\cdot\mathbf{r}/r^3$ we arrive at two separated equations

$$\frac{d^2f_1(\xi)}{d\xi^2} + 2\left(-\frac{I_p(F)}{4} - V_1(\xi,F)\right)f_1(\xi) = 0, \tag{12}$$

$$\frac{d^2f_2(\eta)}{d\eta^2} + 2\left(-\frac{I_p(F)}{4} - V_2(\eta,F)\right)f_2(\eta) = 0. \tag{13}$$

The potentials $V_1$ and $V_2$ are

$$V_1(\xi,F) = -\frac{\beta_1(F)}{2\xi} + \frac{m^2-1}{8\xi^2} + \frac{F\xi}{8}, \tag{14}$$

$$V_2(\eta,F) = -\frac{\beta_2(F)}{2\eta} + \frac{m^2-1}{8\eta^2} - \frac{F\eta}{8} + \frac{\alpha_I F}{\eta^2}, \tag{15}$$

where $\beta_1(F)$ and $\beta_2(F)$ are the separation constants fulfilling

$$\beta_1(F) + \beta_2(F) = Z, \tag{16}$$

$$\beta_2(F) = Z - (1+|m|)\frac{\sqrt{2I_p(F)}}{2}. \tag{17}$$

Again, the potential $V_1(\xi,F)$ along the $\xi$ coordinate is a bound one, while $V_2(\eta,F)$ shows that along the $\eta$ coordinate tunneling is possible. To lowest order in $\xi/\eta$, the potential (14) is identical to the potential obtained for $\xi$ when separating the pure Coulomb plus field problem. In addition to the terms that appear for pure Coulomb potential and a field, the potential (15) along the $\eta$ direction contains the multielectron term $\alpha_I F/\eta^2$. The sum of the separation constants gives the nuclear charge $Z$ [Eq. (16)], in contrast to the FDM where the sum of the separation constants gives the Stark-shifted eigenenergy of the initial state [Eq. (9)].

The separation in parabolic coordinates is not to be understood as a coordinate transformation from the FDM since Eqs. (13) and (8) define different tunneling problems. The tunneling occurs through the $\eta$ coordinate; this defines the geometry of tunneling, that is, the "natural" path of the tunneling current flow in atoms [55]. The tunnel exit point $z_e$ is obtained as $z_e \approx -\eta_e/2$, where $\eta_e$ is obtained by equating the potential $V_2$ of Eq. (15) with the energy term $-I_p/4$, that is,

$$V_2(\eta_e,F) = -\frac{I_p(F)}{4}. \tag{18}$$

The approximate separation of the tunneling problem in parabolic coordinates, together with the inclusion of Stark shifts and the ME term, are the essential ingredients of the TIPIS model. We note that, contrary to the FDM, in this treatment no unphysical assumption about free motion in the transverse degrees of freedom is introduced.

Equation (18) for $\eta_e$ is a cubic equation. However, for exit points that are sufficiently far away from the origin, that is, for

$$\eta_e \gg \frac{2[\alpha_I F + (m^2-1)/8]}{\beta_2(F)}, \tag{19}$$

Eq. (18) becomes quadratic and the exit point $\eta_e$ is well approximated by

$$\eta_e \approx \frac{I_p(F) + \sqrt{I_p^2(F) - 4\beta_2(F)F}}{F}. \tag{20}$$

In Cartesian coordinates, using $z_e \approx -\eta_e/2$,

$$z_e \approx -\frac{I_p(F) + \sqrt{I_p^2(F) - 4\beta_2(F)F}}{2F}, \tag{21}$$

which is different from the corresponding exit point in FDM, following from (5)

$$z_e \approx -\frac{I_p(F) + \sqrt{I_p^2(F) - 4ZF}}{2F}. \tag{22}$$

Below we show examples highlighting that the final momentum depends very sensitively on the use of either Eq. (18) or Eq. (22) for the exit point.

### C. Details of the classical simulations

In our calculations we consider the following short laser pulse elliptically polarized in the $(x,y)$ plane:

$$\mathbf{F}(t) = \frac{F_0}{\sqrt{1+\epsilon^2}} \sin^2(\pi t/\tau_L) \times [\cos(\omega t + \varphi)\mathbf{e}_x + \epsilon \sin(\omega t + \varphi)\mathbf{e}_y], \tag{23}$$

with the duration $\tau_L = (2\pi/\omega)n_p$ and a sine-square envelope, and where $n_p$ is the number of cycles, $\epsilon$ is the ellipticity, and $\varphi$ is the carrier-envelope phase. As in recent experiments [55] we use $\epsilon = 0.78$ throughout. Note that the rescattering process is suppressed for close to circularly polarized field (see, e.g., [71]), and direct electrons, which we are interested in, dominate in the ATI spectrum.

In the present studies we assume that the electron has zero initial velocity in the direction of the laser field $v_{||} = 0$, however, we include an initial transverse velocity $v_{0\perp}$. The ionization instant and this initial transverse velocity are distributed according to the static ionization rate in the tunneling regime [21,22,68]:

$$w(t_0, v_0) \sim \exp\left(-\frac{2\varkappa^3}{3F}\right) \exp\left(-\frac{\varkappa v_{0\perp}^2}{F}\right), \tag{24}$$

where $F = F(t_0)$. For simplicity, we omit the preexponential factor in Eq. (24). Although this factor changes the total ionization rate by several orders of magnitude, its effect on the shape of the final momentum distributions, which we are interested in, is weak for atoms. Moreover, analysis of the transverse momentum distributions in terms of the Siegert eigenfunctions [72] showed that the Gaussian shape of the distribution in Eq. (24) holds if the laser field is less than 0.2 a.u., which is the regime of interest in our case.

An ensemble of $1.5 \times 10^6$ trajectories weighted with the probability given by Eq. (24) was used to calculate the momentum distributions. Equation (1) was solved using a fourth-order Runge-Kutta method with adaptive stepsize control [73]. It is necessary to soften the $1/r^2$ ME term in numerical simulations because it tends to the infinity as $r \to 0$. To do so we multiply this term by the factor $\exp(-b_0/r)$, where $b_0 = 0.1$ a.u. Otherwise, nonphysical bursts can appear in the momentum distributions. Bearing in mind that it is often very difficult to stabilize the carrier-envelope phase in the experiment, we choose $\varphi$ in Eq. (23) randomly for each trajectory. The distributions calculated in this way are, however, very similar to those with $\varphi = \pi$ (or $\varphi = 0$) since the absolute maximum of the field (23) occurs at that particular phase and according to Eq. (24) the absolute maximum of the field is strongly favored. We typically use $n_p = 6$.

The calculation of the momentum distributions of the photoelectrons must take into account the possible population of Rydberg orbits, see [59,74]. So we follow the procedure of Ref. [74] and exclude trajectories with negative energy at the end of the pulse, and take into account the subsequent motion of electrons with positive energies in the Coulomb field of the atomic residual. The electron momentum $\mathbf{q} = \mathbf{q}(t_0, v_0, \tau_L)$ and its position $\mathbf{r} = \mathbf{r}(t_0, v_0, \tau_L)$ at *the end of the laser pulse* uniquely determine the asymptotic momentum:

$$\mathbf{P} = P\frac{P(\mathbf{L}\times\mathbf{a}) - \mathbf{a}}{1 + p^2L^2}. \tag{25}$$

Here $\mathbf{L} = \mathbf{r}\times\mathbf{q}$ and $\mathbf{a} = \mathbf{q}\times\mathbf{L} - \mathbf{r}/r$ are the conserved angular momentum and Runge-Lenz vector, respectively. The above equation corrects a misprint in Ref. [74]. The absolute value $P$ of the asymptotic momentum, appearing in Eq. (25), is found from energy conservation:

$$\frac{q^2}{2} - \frac{Z}{r} = \frac{P^2}{2}. \tag{26}$$

### D. Analytical estimates

Numerical simulations give valuable insights into the properties and evolution of the momentum distributions. Nevertheless, it would be desirable to have some analytical estimates for better understanding of the underlying physics. Let us then write the asymptotic momentum of an electron tunneling at time $t_0$ with nonzero initial velocity $\mathbf{v}_0$ as a sum:

$$\mathbf{P}(t_0, \mathbf{v}_0) = \mathbf{P}_{\rm L}(t_0) + \mathbf{v}_0 + \mathbf{P}_{\rm C}(t_0, \mathbf{v}_0) + \mathbf{P}_{\rm ME}(t_0, \mathbf{v}_0). \tag{27}$$

Here $\mathbf{P}_{\rm C}$ and $\mathbf{P}_{\rm ME}$ are the contributions of the Coulomb force $\mathbf{F}_{\rm C} = -\mathbf{r}/r^3$ and of the multielectron force $\mathbf{F}_{\rm ME} = \nabla[\alpha_I \mathbf{F}(t)\cdot\mathbf{r}/r^3]$, respectively, and $\mathbf{P}_{\rm L}(t_0) = -\int_{t_0}^{\tau_L} \mathbf{F}(t)dt$ is the integral of the force due to the external field $\mathbf{F}(t)$ from the time of ionization. In the simpleman's model $\mathbf{P}_{\rm L}$ is the estimate of the final momentum. Here, however, the effects of other force terms are significant. In order to estimate $\mathbf{P}_{\rm C}$ and $\mathbf{P}_{\rm ME}$, one can use the approach of Refs. [25,74]. Hence we treat the Coulomb and ME potentials as perturbations and calculate each contribution by integrating the respective force along a trajectory $\mathbf{r}_{\rm L}(t) = \int_{t_0}^{t} \mathbf{P}_{\rm L}(t')dt' + \mathbf{v}_0(t - t_0)$ governed by the laser field only:

$$\mathbf{P}_{\rm C} = -\int_{t_0}^{+\infty} dt \frac{\mathbf{r}_{\rm L}(t)}{r_{\rm L}^3(t)}, \tag{28}$$

$$\mathbf{P}_{\rm ME} = \int_{t_0}^{+\infty} dt \left(\frac{\alpha_{\rm I}\mathbf{F}(t)}{r_{\rm L}^3} - \frac{3\alpha_I[\mathbf{F}(t)\cdot\mathbf{r}_{\rm L}]\mathbf{r}_{\rm L}}{r_{\rm L}^5}\right), \tag{29}$$

where the upper integration limit is extended to infinity. We restrict our consideration to sufficiently large ellipticities. Therefore, the trajectory of an electron will not come very close to the atomic residual for the vast majority of initial conditions. Already at the exit of the tunnel the Coulomb and ME forces are small as compared to that of the laser field and they decrease further along the trajectory [25].

Estimates for both contributions can be obtained by calculating the integrals in Eqs. (28) and (29) along the trajectory generated by a constant field $\mathbf{F}(t) = \mathbf{F}(t_0)$. Then, for small initial velocities, $v_0 \ll \varkappa$, the main contributions are given by

$$\mathbf{P}_{\mathrm{C}} = -\frac{\pi}{4}\sqrt{\frac{2}{r_0^3 F(t_0)}}\mathbf{n}_F(t_0) - \frac{v_{0\perp}}{2r_0^2 F(t_0)}\mathbf{n}_\perp(t_0) \tag{30}$$

and

$$\mathbf{P}_{\mathrm{ME}} = \frac{3\pi\alpha_I}{8}\sqrt{\frac{2F(t_0)}{r_0^5}}\mathbf{n}_F(t_0) + \frac{\alpha_I v_{0\perp}}{r_0^3}\mathbf{n}_\perp(t_0), \tag{31}$$

where $r_0$ is the absolute value of the tunnel exit point, $\mathbf{n}_F(t_0)$ is a unit vector along the laser field at time $t_0$, and $\mathbf{n}_\perp(t_0)$ is a unit vector in the polarization plane perpendicular to the laser field at $t_0$.

One can improve the estimate of Eq. (30) by evaluating the integral in Eq. (28) along a trajectory in the field $\mathbf{F}(t) \approx \mathbf{F}(t_0) + \mathbf{F}'(t_0)(t - t_0)$. For simplicity, in this analytical development let us consider only a single electron trajectory, corresponding to the maximum of the field. For such a trajectory and for carrier-envelope phase $\varphi = \pi$ one has $t_0 = \tau_L/2$, and, therefore, $\mathbf{n}_F = \mathbf{e}_x, \mathbf{n}_\perp = \mathbf{e}_y$, and $F = F_0/\sqrt{1+\varepsilon^2}$. Then, one has the following estimate of the Coulomb contribution:

$$\mathbf{P}_{\mathrm{C}}(t_0 = \tau_L/2, v_{0\perp} = 0) = -\left(\frac{\pi}{4}\sqrt{\frac{2}{Fr_0^3}}\mathbf{e}_x + \frac{\epsilon\omega}{6Fr_0}\mathbf{e}_y\right). \tag{32}$$

Let us also introduce the total correction $\mathbf{P}_I = \mathbf{P}_{\mathrm{C}} + \mathbf{P}_{\mathrm{ME}}$ due to the ion potential to the electron momentum:

$$\mathbf{P}_I(t_0 = \tau_L/2, v_{0\perp} = 0) = \frac{\pi}{4}\sqrt{\frac{2}{Fr_0^3}}\left(\frac{3\alpha_I F}{2r_0} - 1\right)\mathbf{e}_x - \frac{\epsilon\omega}{6Fr_0}\mathbf{e}_y. \tag{33}$$

For the parameters considered here $3\alpha_I F/2r_0 \ll 1$ so the estimates Eqs. (32) and (33) show that the contribution of the ME term is small compared to the Coulomb correction. Both contributions increase with increasing intensity, but $\mathbf{P}_{\mathrm{ME}}$ increases faster than $\mathbf{P}_{\mathrm{C}}$ due to the additional factor of $r_0$ in the denominator, see Eq. (33). As we shall see in Sec. III B the estimates provided by Eqs. (32) and (33) underestimate the effect of the ME term and do not account quantitatively for the momentum distributions. However, they do provide valuable insight in the evolution and properties of the momentum distributions.

## III. RESULTS AND DISCUSSION

In the following, using our semiclassical model, we consider the momentum distributions from elliptically polarized pulses, compare them with the solution of the TDSE, and consider the differences between the FDM and TIPIS model. In Ref. [55] the TIPIS model was already compared with experimental data for the rotation (offset) angle of the momentum distribution generated by elliptically polarized field, that is, the angle $\theta$ between the maximum of the distribution and the minor axes of the polarization ellipse. In Fig. 1 we present the momentum distribution in the polarization plane for ionization of Ar by the field of Ti:sapphire laser. The figure shows the main characteristics of the momentum distribution consisting of two main lobes rotated by the angle $\theta$ with respect to the minor axis, and that the distribution peaks at $-\mathbf{A}(t)$.

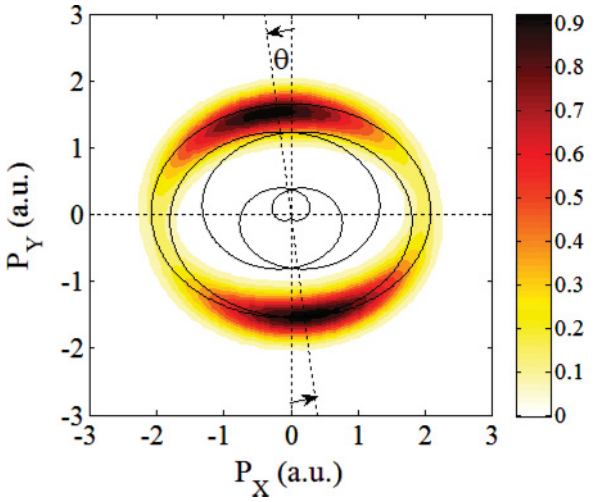


FIG. 1. (Color online) The 2D electron momentum distribution for ionization of Ar by a Ti:sapphire laser pulse ($\lambda = 800$ nm) with a duration $n_p = 6$ cycles, peak intensity of $0.8 \times 10^{15}$ W/cm$^2$, and ellipticity $\epsilon = 0.78$. The Keldysh parameter is $\gamma = 0.5$. The offset angle $\theta$ is shown on the figure. The black curve represents $-\mathbf{A}(t)$, where $\mathbf{A}(t)$ is the vector potential corresponding to the field (23).

### A. Validation of the TIPIS model

We establish the validity of our semiclassical model by comparison with the experiment and an *ab initio* solution of the TDSE. In Fig. 2 we present the momentum distribution in the polarization plane for the case of ionization of the hydrogen atom. In Ref. [75] the solution of the TDSE for the case of the hydrogen atom in a few-cycle circularly polarized laser pulse was presented. The distribution now only has a single main lobe. This is due to the short duration of the phase-stabilized pulse. Calculations in our semiclassical model for the exact same parameters as in Ref. [75] yielded the momentum distribution in Fig. 2. Comparing the momentum distributions obtained with the TDSE, the distributions in Fig. 2 look qualitatively very similar. The interference pattern that is present in the TDSE momentum distribution is not reproducible by our semiclassical model. A quantitative comparison of the distributions can be made by calculating the offset angle: for the TDSE the offset angle is 23° for $5.0 \times 10^{13}$ W/cm$^2$ and 12° for $10^{14}$ W/cm$^2$ [75], while the offset angles calculated at these intensities within the semiclassical model are 18° and 15°, respectively. The agreement is quite good, also for lower intensity where $\gamma = 1.5$, and the application of tunneling

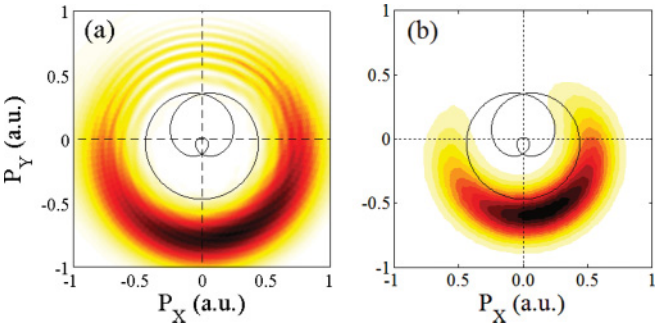


FIG. 2. (Color online) The 2D electron momentum distributions in the polarization plane for ionization of H(1$s$) by circularly polarized Ti:sapphire laser pulse with a duration $n_p = 3$ cycles and peak intensity of $10^{14}$ W/cm$^2$. Panels (a) and (b) show results obtained by solving the TDSE, and using the classical simulations within the TIPIS model, respectively. The curves represent $-\mathbf{A}(t)$, where $\mathbf{A}(t)$ is the vector potential, defined as in Ref. [75] for this particular figure.

theory for the description of the initial tunneling step is expected to be less accurate.

### B. Momentum distributions for λ = 1600 and λ = 800 nm: Difference between the FDM and the TIPIS model, and the role of the ME term

We are interested in a situation where the offset angle $\theta$ is larger than for noble gases, that is, when the rotation of the momentum distribution is more pronounced, so that any differences between the semiclassical approaches and also the role of the ME term could be more easily observed. At first glance it would seem that alkali metals are suitable candidates for a large $\theta$. Indeed, the static polarizabilities of the Ar and $Ar^+$ atom are $\alpha_N = 11.08$ a.u. and $\alpha_I = 7.2$ a.u, and, for example, in the case of Li the same quantities are equal to 164.2 and 0.1883 a.u., respectively [76,77]. However, alkali metals have very low ionization potential (for Li $I_0 = 5.39$ eV) and this prevents us from using them in our simulations. In order to understand this fact, let us discuss the applicability conditions of the TIPIS model in more detail.

The validity range of the simulations based on the TIPIS approach is restricted by the two following conditions. On one hand, the laser intensity should not be too high: The second term of Eq. (3) should be not more than 10−20% of the first one. On the other hand, the laser field needs to be strong enough to keep the Keldysh parameter less than or of the order of unity, such that the ionization probability can be described by tunneling. Thus for each atomic species and given wavelength (in our case $\lambda = 1600$ or $\lambda = 800$ nm) the aforementioned conditions define a range of acceptable intensities. In the case of Li and $\lambda = 800$ nm, this range of intensities is $8.7 \times 10^{12}$−$8.7 \times 10^{13}$ W/cm$^2$, which corresponds to the following interval of the Keldysh parameter: $\gamma = 4.8 - 1.6$. Although the tunneling ionization rate often works even when the Keldysh parameter is several times greater than unity (see, e.g., Ref. [78]), we do not consider alkali metals here.

A close inspection of the ionization potentials and static polarizabilities of different atomic species shows that elements as Mg, Cu, or Zn can be used for the present purpose. Indeed, these elements have higher ionization potentials than the alkali metals. Simultaneously, their polarizabilities are high and substantially different from those of the corresponding ions. We perform our simulations for Mg since multiphoton ionization of this atom has already attracted attention in experiment [79–83] and theory [84–88]. For Mg, $I_p = 0.28$ a.u., $\alpha_N = 71.33$ a.u., and $\alpha_I = 35.00$ a.u., and at the wavelength of 800 nm, our simulation technique is applicable at the intensities of $2.35 \times 10^{13}$−$1.0 \times 10^{14}$ W/cm$^2$, for which the Keldysh parameter is $\gamma = 2.0 - 1.0$.

The results of our simulations for Mg are shown in Figs. 3–5. First we turn our attention to Figs. 3 and 4 where 2D momentum distributions at three different intensities calculated within three different semiclassical models at two wavelengths are shown. The difference between the semiclassical models compared in Figs. 3 and 4 is the potential $V(\mathbf{r})$ in which the classical trajectories (1) are propagated. The first column of Figs. 3 and 4, that is, panels (a), (d), and (g), presents the distributions, calculated ignoring the influence of the ionic potential on the electron motion after tunneling, that is, the tunneled electron moves only in the laser field (the simpleman's model). It is reasonable therefore that these distributions are very similar to those obtained within the SFA (see, e.g. Ref. [78]). The second column of Figs. 3 and 4 shows the same distributions, but now including the Coulomb potential. Finally, the third column presents the results of the full TIPIS model when an electron moves under the action of the laser field and the potential of Eq. (4). It should be stressed that in all three cases the exit points were calculated with the account of the Stark shift, while for the distributions in the first and the second columns of Figs. 3 and 4, the ME term was omitted in Eq. (18). Moreover, the effect of the capture into Rydberg states was taken into account while calculating the distributions of Figs. 3 and 4, see Sec. II above.

The distributions of Fig. 3 are similar to those for Ar at 800 nm, see Fig. 1 and Ref. [55]. As expected, the effect of the rotation is more pronounced, now $\theta \in [30°; 40°]$, whereas for Ar it was $\theta \in [10°; 15°]$ (see Fig. 1). At the same intensities the shape of the distributions at a wavelength of 800 nm differs from that at a wavelength of 1600 nm, compare Fig. 3 and Fig. 4. The reason is that the Keldysh parameter at $\lambda =$ 800 nm is two times greater than at $\lambda = 1600$ nm. This, in turn, has two consequences. First, for larger $\gamma$ the 2D distribution calculated within the plain SM [see Figs. 4(a), 4(d), and 4(g)] is two times closer to the origin of the $(p_x, p_y)$ plane because one has $\mathbf{P} = \mathbf{P}_L \sim (F/\omega, \epsilon F/\omega) = (\varkappa/\gamma, \epsilon\varkappa/\gamma)$. Conversely, at $\lambda = 800$ nm the relative yield of neutral excited atoms $N^*$ with respect to the number of singly charged ions $N^+$ is larger than at a wavelength of 1600 nm in accordance with Ref. [74], where $N^*/N^+ \sim 1/\lambda^{5/2}$, provided the field strength $F$ is the same for the two wavelengths.

In the first column of Figs. 3 and 4 the momentum distributions consist of two lobes along the minor polarization axis (along the $P_y$ axis), that peak at $P_y$ equal to the value of the vector potential at the time of maximum emission [the time when the electric field (23) points along the major polarization axis]. In the second and third columns of Figs. 3 and 4, the momentum distributions are shifted with respect to the minor polarization axis of the field by some offset angle, discussed above in connection with Fig. 1. By comparison between the second and third columns in Figs. 3 and 4 we

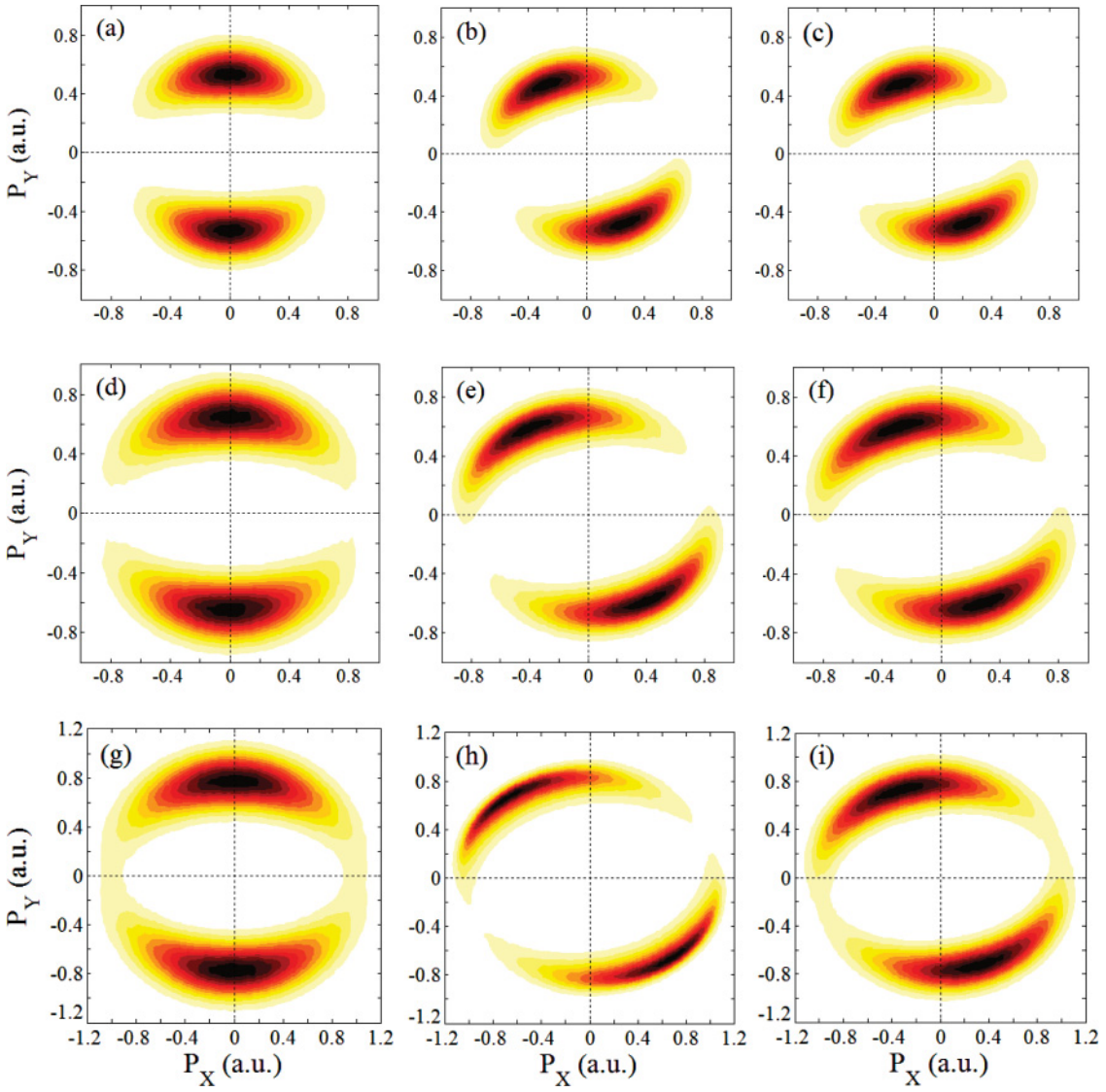


FIG. 3. (Color online) Momentum distributions of the photoelectrons emitted from Mg at a wavelength of 1600 nm and ellipticity $\epsilon = 0.78$ calculated within the three different versions of semiclassical approaches. The left column, that is, panels (a), (d), and (g), shows the distributions, calculated ignoring the ionic potential after tunneling, when the tunneled electron moves in the laser field only. The middle column [panels (b), (e), and (h)] depicts the same distributions, but with consideration for the Coulomb field. The right column [panels (c), (f), and (i)] presents the results of the full TIPIS model, when both terms are taken into account in Eq. (4). The distributions (a)–(c), (d)–(f), and (g)–(i) correspond to the intensity of 2.35, 3.5, and $5.0 \times 10^{13}$ W/cm$^2$, and to the Keldysh parameter of 1.05, 0.85, and 0.7, respectively. The same color scale is used for all the distributions.

can gauge the influence of the ME term. At low intensities [Figs. 3(b), 3(c), 4(b), and 4(c)] the ME term does not play any noticeable role: there is hardly any difference whether the ME term is taken into account or not. However, the situation changes with increasing intensity: The offset angles $\theta$ of the distributions of Figs. 3(f) and 3(i) are smaller than those of Figs. 3(e) and 3(h). This is so because in the initial stages of the propagation the ME and Coulomb forces act in opposite directions, which results in a smaller offset angle when the ME term is taken into account. This feature is also captured in the analytic estimates: the $x$ components of the Coulomb and ME corrections of the electron momentum have different signs, see Eq. (33). Next, detailed comparison of the semiclassical calculations and the analytic estimates show that the estimate of Eq. (31) for the contribution of the ME term is quite good. For example, at the intensity of $5.0 \times 10^{13}$ W/cm$^2$ and at a wavelength of 800 nm, for $\varphi = \pi$ and $I_p = 7.64$ eV (Mg atom), and for initial conditions, which correspond to the maximum of the field Eq. (23), that is, for $t_0 = \tau_L/2$ and $\mathbf{v}_0 = 0$, one has $\mathbf{P}_{\rm ME} = (0.058, 0)$ from the estimate Eq. (31), whereas exact numerical solution of Newton's equations gives $(0.046, -0.01)$. Contrary to this, the estimate of the Coulomb contribution Eq. (30) is not accurate. The latter does not describe a decrease in the $P_y$ component due to the Coulomb field (along minor axis), see Fig. 4, which is clear from the following example: For the same initial conditions and field parameters as above, the estimate Eq. (30) gives $\mathbf{P}_{\rm C} = (-0.27, 0)$, whereas the numerical solution gives

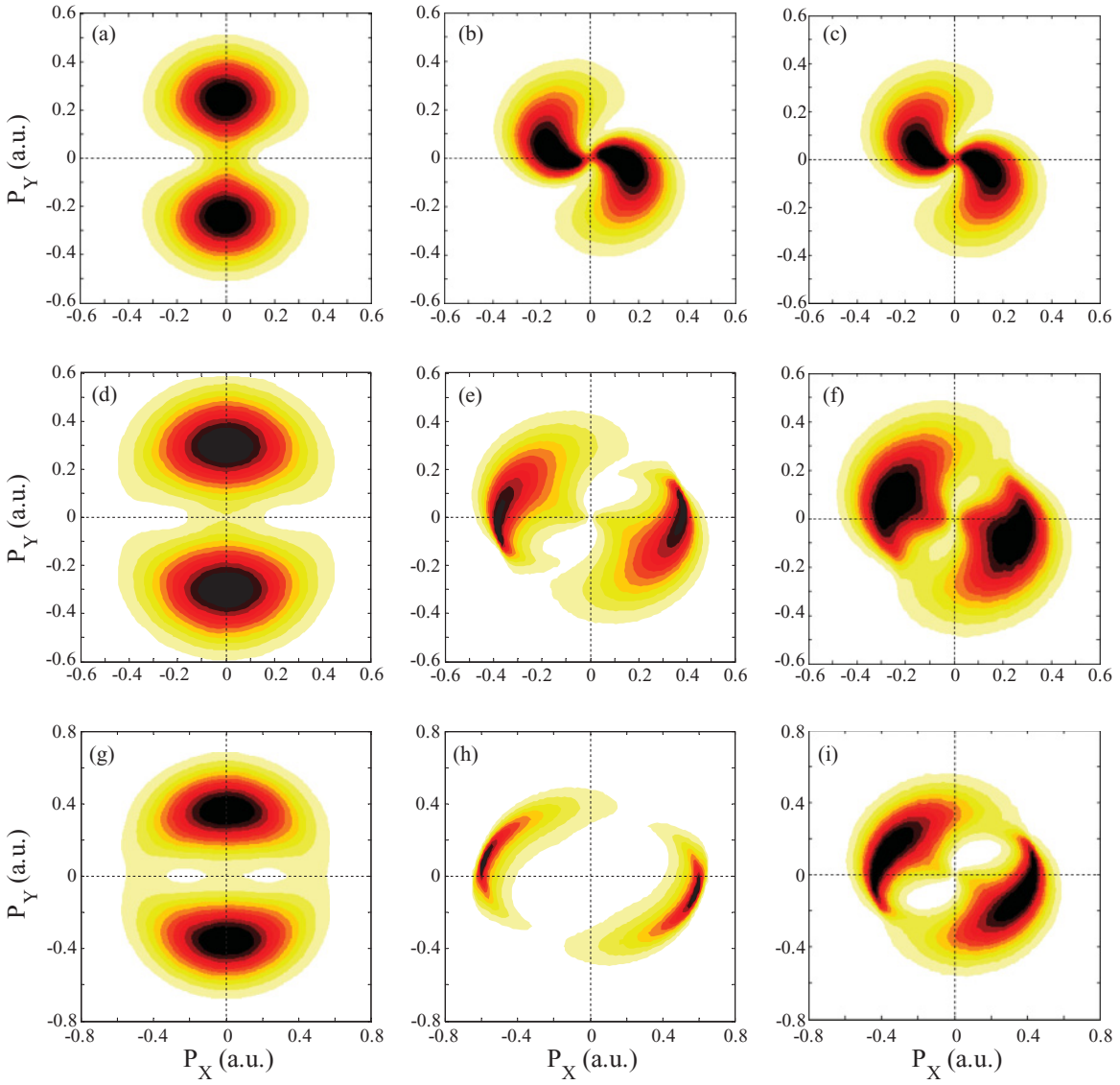


FIG. 4. (Color online) Momentum distributions of the photoelectrons emitted from Mg at a wavelength of 800 nm and ellipticity $\epsilon = 0.78$ calculated within the three different versions of semiclassical approaches. The left column, that is, panels (a), (d), and (g), shows the distributions, calculated ignoring the ionic potential after tunneling, when the tunneled electron moves in the laser field only. The middle column [panels (b), (e), and (h)] depicts the same distributions, but with consideration for the Coulomb field. The right column [panels (c), (f), and (i)] presents the results of the full TIPIS model, when both terms are taken into account in Eq. (4). The distributions (a)–(c), (d)–(f), and (g)–(i) correspond to the intensity of 2.35, 3.5, and $5.0 \times 10^{13}$ W/cm$^2$, and to the Keldysh parameter of 2.1, 1.7, and 1.4, respectively. The same color scale is used for all the distributions.

$(-0.31, -0.19)$ with a nonvanishing $y$ component. Therefore the estimate of Eq. (32) is to be used instead of Eq. (30).

The evolution of the distributions at $\lambda = 800$ nm with increasing intensity is more dramatic since not only do the angular offset changes, but also the shapes of the momentum distributions. The two main lobes in the momentum distribution, although distorted, are still present, but also a substantial amount of probability is located in the low-energy part of the distribution. The central (low energy) part of the distribution shown in Fig. 4(e) is more depleted than that of Fig. 4(f). One could expect that this depletion results from the more effective capture into bound states in the absence of the ME force. This is, however, not true. From the estimate (33) one can see that the magnitude of the final electronic momentum is slightly decreased when the ME term is taken into account. This leads to a larger number of electronic trajectories finishing with smaller radial momenta and, in accord with Eq. (26), more trajectories will finish with negative energy and be captured. Hence the effect of capture after the end of the pulse is stronger when the ME term is taken into account in the potential of Eq. (4): The relative yields of the captured trajectories associated with the momentum distributions of Figs. 4(e) and 4(f) are equal to 0.06 and 0.13, respectively. As expected from Eq. (15), it is seen from Figs. 3 and 4 that the influence of the ME term increases with increasing intensity, which is again consistent with the estimate of Eq. (31).

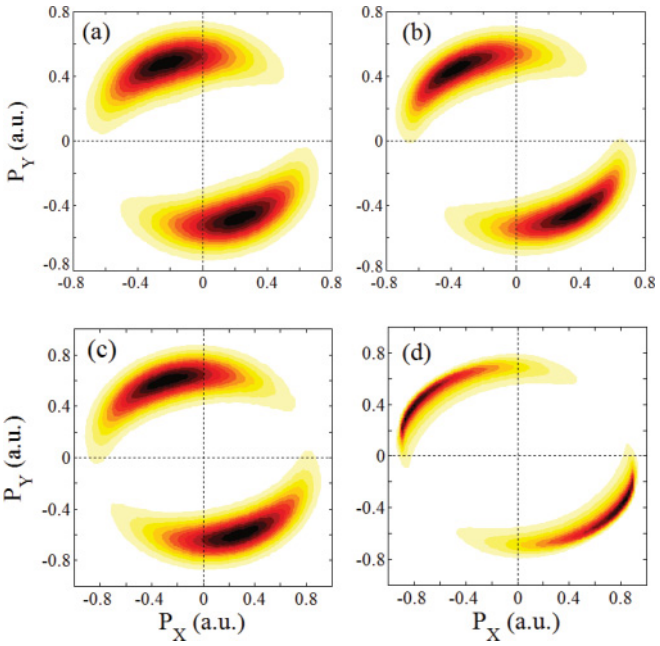


FIG. 5. (Color online) The electron momentum distributions for ionization of Mg at a wavelength of 1600 nm for the ellipticity $\epsilon = 0.78$ and two different intensities: (a), (b) $2.35 \times 10^{13}$ W/cm$^2$ and (c), (d) $3.5 \times 10^{13}$ W/cm$^2$, which corresponds to the Keldysh parameter $\gamma$ of 1.05 and 0.85, respectively. The left column of the panels corresponds to the TIPIS model, whereas the right one presents the results of the FDM with the potential given by Eq. (4). In both cases Stark shifts and ME terms are included. The color scale is the same for all the panels.

Next we test to which extent the separation procedure of the static problem of an atom plus field into an one-dimensional tunneling problem, described in Secs. II A and II B, can influence the outcome of the semiclassical simulation. Momentum distributions calculated according to the full TIPIS approach and within the FDM with all force terms are shown in Fig. 5 for three different laser intensities at wavelengths of 1600 nm. The only difference between these approaches is the position of the exit point, which is different in TIPIS and in FDM. We note that in all cases in Fig. 5 the tunneling occurs below the barrier, calculated in FDM or TIPIS. Figure 5 illustrates that the exit point plays a crucial role in semiclassical simulations.

Since $\beta_2(F) < Z$ [see Eq. (17)], and comparing Eqs. (21) and (22), it is evident that the exit point evaluated with the TIPIS model is larger than in the FDM. This is true whether the inequality Eq. (19) is valid (as in the case of Figs. 3–5) or not. Smaller exit points result in larger influence of the parent ion potential on the trajectory of the tunnelled electron and therefore larger offset angle. This explains why the offset angle is larger in the FDM. At the lower intensity [Figs. 5(a) and 5(b)], the difference between the exit points in the FDM and the TIPIS model is small and therefore the differences between the momentum distributions [Figs. 5(a) and 5(b)] are small. Increasing the intensity [Figs. 5(c) and 5(d)], the tunnel exit point moves closer to the origin and simultaneously the difference between the exit points obtained with the FDM and the TIPIS model increases. Hence, there is a large difference between the offset angles in Figs. 5(c) and 5(d). These trends are correctly captured in the analytic estimates (30)–(31) and (33): they are all inverse proportional to powers of the tunnel exit point $r_0$. In the final expression of Eq. (33), the ratio between the $x$ and the $y$ component of final momentum is inverse proportional to the tunnel exit point, which gives correct dependence of the offset angle on the tunnel exit point.

## IV. CONCLUSIONS

In conclusion, we have investigated in detail a recently introduced physical picture of above-threshold ionization [55]: Tunnel ionization in parabolic coordinates with induced dipole and Stark shift followed by classical propagation in all force fields. We have tested this model by applying it for the investigation of the photoelectron momentum distributions in elliptically polarized field. The present approach demonstrates good agreement with recent experimental data [55] and with TDSE [75]. The role of the multielectron effects in the formation of the photoelectron momentum distributions is clearly identified and investigated over a wide range of laser intensities and wavelengths. The tunnel exit point, and with it the separation procedure yielding the one-dimensional tunneling problem, are clearly demonstrated to have a profound influence on the momentum distributions. The evolution of the momentum distributions with respect to the intensity, the terms in the atomic (ionic) potential, and the tunnel exit point are correctly captured by the analytic estimates and scalings proposed here. Finally, all the effects presented here are studied using pulses with random carrier-envelope phase and therefore can be easily checked in an experiment.

## ACKNOWLEDGMENTS

This work was supported by the Danish Research Council (Grant No. 10-085430), the ERC-2011-StG (Project No. 277767), and partially supported by the Russian Foundation of Basic Research (Project No. 09-02-00773-a), as well as by the Federal Goal Program (Project No. P1546).

[1] M. V. Fedorov, *Atomic and Free Electrons in a Strong Laser Field* (World Scientific, Singapore, 1997).
[2] N. B. Delone and V. P. Krainov, *Multiphoton Processes in Atoms* (Springer, Berlin, 2000), Chap. 9.
[3] W. Becker, F. Grasbon, R. Kopold, D. B. Milošević, G. G. Paulus, and H. Walther, Adv. At. Mol. Opt. Phys. **48**, 35 (2002).
[4] D. B. Milošević and F. Ehlotzky, Adv. At. Mol. Opt. Phys. **49**, 373 (2003).
[5] A. Becker and F. H. M. Faisal, J. Phys. B **38**, R1 (2005).
[6] C. Figueira de Morisson Faria and X. Liu, J. Mod. Opt. **58**, 1076 (2011).
[7] E. Cormier and P. Lambropoulos, J. Phys. B **30**, 77 (1997).

[8] M. Nurhuda and F. H. M. Faisal, Phys. Rev. A **60**, 3125 (1999).
[9] H. G. Muller, Laser Phys. **9**, 138 (1999).
[10] D. Bauer and P. Koval, Comput. Phys. Commun. **174**, 396 (2006).
[11] T. K. Kjeldsen, Ph.D. thesis, University of Århus, Århus, Denmark, 2007.
[12] L. V. Keldysh, Zh. Eksp. Teor. Fiz. **47**, 1945 (1964) [Sov. Phys. JETP **20**, 1307 (1965)].
[13] F. H. M. Faisal, J. Phys. B **6**, L89 (1973).
[14] H. R. Reiss, Phys. Rev. A **22**, 1786 (1980).
[15] H. B. van Linden van den Heuvell and H. G. Muller, in *Multiphoton Processes*, edited by S. J. Smith and P. L. Knight (Cambridge University Press, Cambridge, 1988).
[16] T. F. Gallagher, Phys. Rev. Lett. **61**, 2304 (1988).
[17] P. B. Corkum, N. H. Burnett, and F. Brunel, Phys. Rev. Lett. **62**, 1259 (1989).
[18] K. C. Kulander, K. J. Schafer, and J. L. Krause, in *Super-Intense Laser-Atom Physics*, edited by B. Piraux, A. L'Hullier, and K. Rzazewski (Plenum, New York, 1993).
[19] P. B. Corkum, Phys. Rev. Lett. **71**, 1994 (1993).
[20] L. D. Landau and E. M. Lifschitz, *Quantum Mechanics Non-relativistic Theory*, 2nd ed. (Pergamon, Oxford, 1965).
[21] A. M. Perelomov, V. S. Popov, and M. V. Terent'ev, Zh. Eksp. Teor. Fiz. **50**, 1393 (1966) [Sov. Phys. JETP **23**, 924 (1966)].
[22] M. V. Ammosov, N. B. Delone, and V. P. Krainov, Zh. Eksp. Teor. Fiz. **91**, 2008 (1986) [Sov. Phys. JETP **64**, 1191 (1986)].
[23] M. Bashkansky, P. H. Bucksbaum, and D. W. Schumacher, Phys. Rev. Lett. **60**, 2458 (1988).
[24] G. G. Paulus, F. Grasbon, A. Dreischuh, H. Walther, R. Kopold, and W. Becker, Phys. Rev. Lett. **84**, 3791 (2000).
[25] S. P. Goreslavski, G. G. Paulus, S. V. Popruzhenko, and N. I. Shvetsov-Shilovski, Phys. Rev. Lett. **93**, 233002 (2004).
[26] S. Basile, F. Trombetta, and G. Ferrante, Phys. Rev. Lett. **61**, 2435 (1988).
[27] P. Lambropoulos and X. Tang, Phys. Rev. Lett. **61**, 2506 (1988).
[28] H. G. Muller, G. Petite, and P. Agostini, Phys. Rev. Lett. **61**, 2507 (1988).
[29] S. V. Popruzhenko and D. Bauer, J. Mod. Opt. **55**, 2573 (2008).
[30] S. V. Popruzhenko, G. G. Paulus, and D. Bauer, Phys. Rev. A **77**, 053409 (2008).
[31] T.-M. Yan, S. V. Popruzhenko, M. J. J. Vrakking, and D. Bauer, Phys. Rev. Lett. **105**, 253002 (2010).
[32] A. Emmanouilidou and D. S. Tchitchekova, Phys. Rev. A **84**, 033407 (2011).
[33] N. I. Shvetsov-Shilovski, S. P. Goreslavski, S. V. Popruzhenko, and W. Becker, Phys. Rev. A **77**, 063405 (2008).
[34] X. Wang and J. H. Eberly, Phys. Rev. Lett. **103**, 103007 (2009).
[35] X. Wang and J. H. Eberly, Phys. Rev. Lett. **105**, 083001 (2010).
[36] X. Wang and J. H. Eberly, New J. Phys. **12**, 093047 (2010).
[37] F. Mauger, C. Chandre, and T. Uzer, Phys. Rel. Lett. **105**, 083002 (2010).
[38] G. G. Paulus, F. Grasbon, H. Walther, P. Villoresi, M. Nisoli, S. Stagira, E. Priori, and S. De. Silvestri, Nature (London) **414**, 182 (2001).
[39] D. B. Milošević, G. G. Paulus, and W. Becker, Phys. Rev. Lett. **89**, 153001 (2002).
[40] D. B. Milošević, G. G. Paulus, and W. Becker, Laser Phys. **13**, 948 (2003).
[41] A. M. Perelomov, V. S. Popov, and M. V. Terent'ev, Zh. Eskp. Teor. Fiz. **51**, 309 (1966) [Sov. Phys. JETP **24**, 207 (1967)].
[42] P. Krstic and M. H. Mittleman, Phys. Rev. A **44**, 5938 (1991).
[43] A. Jaron, J. Z. Kaminski, and F. Ehlotzky, Opt. Commun. **163**, 115 (1999).
[44] N. L. Manakov, M. V. Frolov, B. Borca, and A. F. Starace, J. Phys. B **33**, R141 (2000).
[45] S. P. Goreslavski and S. V. Popruzhenko, Zh. Eksp. Teor. Fiz. **110**, 1200 (1996) [Sov. Phys. JETP **83**, 661 (1996)].
[46] G. G. Paulus, F. Zacher, H. Walther, A. Lohr, W. Becker, and M. Kleber, Phys. Rev. Lett. **80**, 484 (1998).
[47] M. Busuladžić, A. Gazibegović-Busuladžić, and D. B. Milošević, Phys. Rev. A **80**, 013420 (2009).
[48] M. Busuladžić, A. Gazibegović-Busuladžić, and D. B. Milošević, Laser Phys. **20**, 1001 (2010).
[49] L. Holmegaard, J. L. Hansen, L. Kalhøj, S. L. Kragh, H. Stapelfeldt, F. Filsinger, J. Küpper, G. Meijer, D. Dimitrovski, M. Abu-samha, C. P. J. Martiny, and L. B. Madsen, Nat. Phys. **6**, 428 (2010).
[50] D. Dimitrovski, M. Abu-samha, L. B. Madsen, F. Filsinger, G. Meijer, J. Küpper, L. Holmegaard, L. Kalhøj, J. H. Nielsen, H. Stapelfeldt, Phys. Rev. A **83**, 023405 (2011).
[51] J. L. Hansen, L. Holmegaard, L. Kalhøj, S. L. Kragh, H. Stapelfeldt, F. Filsinger, G. Meijer, J. Küpper, D. Dimitrovski, M. Abu-samha, C. P. J. Martiny, and L. B. Madsen, Phys. Rev. A **83**, 023406 (2011).
[52] J. L. Hansen and H. Stapelfeldt, D. Dimitrovski, M. Abu-samha, C. P. J. Martiny, and L. B. Madsen, Phys. Rev. Lett. **106**, 073001 (2011).
[53] P. Eckle, A. N. Pfeiffer, C. Cirelli, A. Staudte, R. Dörner, H. G. Muller, M. Büttiker, and U. Keller, Science **322**, 1525 (2008).
[54] P. Eckle, M. Smolarski, P. Schlup, J. Biegert, A. Staudte, M. Schöffler, H. G. Muller, R. Dörner, and U. Keller, Nat. Phys. **4**, 565 (2008).
[55] A. N. Pfeiffer, C. Cirelli, M. Smolarski, D. Dimitrovski, M. Abu-samha, L. B. Madsen, and U. Keller, Nat. Phys. **8**, 76 (2012).
[56] D. Dimitrovski, C. P. J. Martiny, and L. B. Madsen, Phys. Rev. A **82**, 053404 (2010).
[57] T. Brabec, M. Yu. Ivanov, and P. B. Corkum, Phys. Rev. A **54**, R2551 (1996).
[58] J. Chen and C. H. Nam, Phys. Rev. A **66**, 053415 (2002).
[59] T. Nubbemeyer, K. Gorling, A. Saenz, U. Eichmann, and W. Sandner, Phys. Rev. Lett. **101**, 233001 (2008).
[60] C. Liu and K. Z. Hatsagortsyan, J. Phys. B **44**, 095402 (2011).
[61] C. Liu and K. Hatsagortsyan, e-print arXiv: 1109.5645v1 [physic.atom-ph] (2011).
[62] A. Kästner, U. Saalmann, and J. M. Rost, Phys. Rev. Lett. **108**, 033201 (2012).
[63] C. Lemell, K. I. Dimitriou, X.-M. Tong, S. Nagele, D. V. Kartashov, J. Burgdörfer, and S. Gräfe, Phys. Rev. A **85**, 011403(R) (2012).
[64] A. Kästner, U. Saalmann, and J. M. Rost, Phys. Rev. Lett. **108**, 033201 (2012).
[65] J. Chen, J. Liu, L. B. Fu, and W. M. Zheng, Phys. Rev. A **63**, 011404(R) (2000).
[66] L. B. Fu, J. Liu, J. Chen, and S. G. Chen, Phys. Rev. A **63**, 043416 (2001).
[67] T. Brabec, M. Côté, P. Boulanger, and L. Ramunno, Phys. Rev. Lett. **95**, 073001 (2005).
[68] N. B. Delone and V. P. Krainov, J. Opt. Soc. Am. B **8**, 1207 (1991).

[69] K. I. Dimitriou, D. G. Arbo, S. Yoshida, E. Persson, and J. Burgdörfer, Phys. Rev. A **70**, 061401(R) (2004).
[70] M. Yu. Ivanov, M. Spanner, and O. Smirnova, J. Mod. Opt. **52**, 165 (2005).
[71] M. Abu-samha and L. B. Madsen, Phys. Rev. A **84**, 023411 (2011).
[72] P. A. Batishchev, O. I. Tolstikhin, and T. Morishita, Phys. Rev. A **82**, 023416 (2010).
[73] W. H. Press, S. A. Teukolsky, W. T. Vetterling, and B. P. Flannery, *Numerical Recipes in Fortran 77: The Art of Scientific Computing*, 2nd ed. (Cambridge University Press, Cambridge, 1992).
[74] N. I. Shvetsov-Shilovski, S. P. Goreslavski, S. V. Popruzhenko, and W. Becker, Laser Phys. **19**, 1550 (2009).
[75] C. P. J. Martiny, M. Abu-samha, and L. B. Madsen, J. Phys. B **42**, 161001 (2009).
[76] J. Mitroy, M. S. Safronova, and C. W. Clark, J. Phys. B **43**, 202001 (2010).
[77] M. P. F. Bristow and I. I. Glas, Phys. Fluids **15**, 2066 (1972).
[78] V. S. Popov, Usp. Fiz. Nauk **174**, 921 (2004) [Phys. Usp. **47**, 855 (2004)].
[79] D. Kim, S. Fournier, M. Saeed, and L. F. DiMauro, Phys. Rev. A **41**, 4966 (1990).
[80] N. J. van Druten, R. Trainham, and H. G. Muller, Phys. Rev. A **50**, 1593 (1994).
[81] D. Xenakis, N. E. Karapanagioti, D. Charalambidis, and H. Bachau, and E. Cormier, Phys. Rev. A **60**, 3916 (1999).
[82] G. D. Gillen, M. A. Walker, and L. D. Van Woerkom, Phys. Rev. A **64**, 043413 (2001).
[83] G. D. Gillen and L. D. Van Woerkom, Phys. Rev. A **68**, 033401 (2003).
[84] J. Zhang and P. Lambropoulos, Phys. Rev. Lett. **77**, 2186 (1996).
[85] L. A. A. Nikolopoulos, G. Buica-Zloh, and P. Lambropoulos, Eur. Phys. J. D **26**, 245 (2003).
[86] I. Liontos, A. Bolovinos, S. Cohen, and A. Lyras, Phys. Rev. A **70**, 033403 (2004).
[87] T. Nakajima and G. Buica, Phys. Rev. A **74**, 023411 (2006).
[88] G. Buica and T. Nakajima, Phys. Rev. A **79**, 013419 (2009).